RSC Advances

PAPER

Cite this: *RSC Adv.*, 2024, **14**, 15755

Identification of acetaldehyde based on plasmonic patterns of a gold nanostructure conjugated with chromophore and H_2O_2: a new platform for the rapid and low-cost analysis of carcinogenic agents by colorimetric affordable test strip (CATS)†

Fatemeh Farshchi,[a] Arezoo Saadati,‡[b] Farnaz Bahavarnia,[c] Mohammad Hasanzadeh *[d] and Nasrin Shadjou [e]

Acetaldehyde, a prevalent carbonyl compound in fermented foods, poses challenges in various applications due to its reactivity. This study addresses the need for efficient acetaldehyde detection methods across biotechnological, environmental, pharmaceutical, and food sectors. Herein, we present a novel colorimetric/UV spectrophotometric approach utilizing gold nanoparticles (AuNPs), particularly gold nano-flowers (AuNFs), for sensitive acetaldehyde identification. The method exhibits a notable sensitivity, detecting acetaldehyde at concentrations as low as 0.1 μM. The mechanism involves the interaction of acetaldehyde molecules with AuNFs, leading to a significant change in the absorbance spectrum, which serves as the basis for detection. Moreover, its applicability extends to human biofluids, notably urine samples. Integration with a cost-effective one-drop microfluidic colorimetric device (OD-μPCD) enables the development of an affordable test strip (CATS). This semi-analytical device, employing a multichannel OD-μPCD, facilitates real-time analysis of acetaldehyde in human samples. Our findings demonstrate the pioneering utilization of AuNPs for selective and sensitive acetaldehyde detection, promising advancements in environmental and occupational safety standards, and laying a foundation for enhanced detection and monitoring of related volatile organic compounds (VOCs).

Received 16th April 2024
Accepted 3rd May 2024

DOI: 10.1039/d4ra02814g

rsc.li/rsc-advances

1. Introduction

The presence of various toxins in the environment poses significant risks to human health and underscores the necessity for rapid and accurate detection methods.[1] Among these toxins, acetaldehyde, commonly found in food and air, is particularly concerning due to its carcinogenic properties.[2–4] Designated as a Group I carcinogen by the International Agency for Research on Cancer (IARC), acetaldehyde underscores the importance of monitoring food safety and air pollution.[5] Consequently, there is a pressing need for simple and sensitive methods to detect acetaldehyde in specific biotechnological processes, environmental management, pharmaceuticals, and even in the analysis of drinking water and food.[6]

Analytical techniques like HPLC and GC have been utilized for acetaldehyde detection.[7] While they offer valuable insights, their intricate derivatization processes and prolonged detection times hinder immediate determination.[8] In the realm of metal oxides, zinc oxide (ZnO) has shown promise in detecting volatile organic compounds (VOCs) effectively. Efforts to enhance ZnO's capabilities include structural modifications like shaping it into flower-like structures to increase surface area.[9] Additionally, combining different metal oxides, such as PdO–ZnO P–N heterojunction nanostructures, has demonstrated sensitivity and selectivity in acetaldehyde detection. Doping ZnO with elements like cobalt (Co) has expanded its detection range.[10] These methods are also complicated and require special laboratory equipment.

The incorporation of these technologies into microfluidic platforms holds potential for new systems that can be marketed as diagnostic tools.[11,12] This type of sensor enables simultaneous detection of diverse parameters.[13,14] A widely recognized approach is to employ paraffin wax and metal molds, known for their flexibility and ease of fabrication. These materials remain

[a]*Fundação Oswaldo Cruz, Instituto Oswaldo Cruz, Laboratório de Biologia Molecular e Doenças Endêmicas, Avenida Brasil No 4365-Manguinhos, Rio de Janeiro 21040-900, Brazil*

[b]*Central European Institute of Technology, Brno University of Technology, Brno CZ-612 00, Czech Republic*

[c]*Nutrition Research Center, Tabriz University of Medical Sciences, Tabriz, Iran*

[d]*Pharmaceutical Analysis Research Center, Tabriz University of Medical Sciences, Tabriz, Iran. E-mail: hasanzadehm@tbzmed.ac.ir*

[e]*Department of Nanotechnology, Faculty of Chemistry, Urmia University, Urmia, Iran*

† Electronic supplementary information (ESI) available. See DOI: https://doi.org/10.1039/d4ra02814g

‡ Co-first author.

in demand and are commercially viable due to their cost-effectiveness.[15]

One of the most widely adopted methods for colorimetric analysis involves leveraging gold nanoparticles (AuNPs) as indicators, effectively enhancing system precision and sensitivity. The unique properties of AuNPs, including their localization of plasmonic bands and ease of synthesis, render them extensively used in biomedical applications.[16] Moreover, nanoparticle characteristics make them an excellent platform for biological analysis, impacting optical properties based on size and shape variations, thereby enhancing diagnostic sensitivity.[17,18] Advancements in spectroscopic technology have facilitated the development of optical sensors for acetaldehyde detection, including microfluidic sensors based on colorimetry.[19] Despite the utility of colorimetric-based sensors, challenges such as the need for trained personnel, limited resolution, and complex procedures persist.[19] Consequently, researchers are exploring modifications to existing technologies or investigating novel diagnostic methods to design cost-effective, dependable, disposable laboratories that operate independently of electrical connections.[20]

To execute chemical reactions using simple and cost-effective methods, microfluidic systems have been suggested.[21] Paper-based microfluidic designs, utilizing hydrophobic barriers to form hydrophilic channels, offer portability and versatility, suitable for various settings.[22,23] This study presents a novel diagnostic platform for rapid and accurate detection of acetaldehyde using UV-visible spectroscopy and colorimetric analysis.[24] Various types of AuNPs with different shapes and pH values were initially employed as analytes, establishing a reliable colorimetric method in combination with UV-visible spectroscopy for identifying acetaldehyde in real samples. Integrated with an optimized one-droplet microfluidic glass fiber-based device (OD-μPCD), the system offers semi-quantitative results. The study utilized glass fiber paper to manufacture microfluidic wafers, demonstrating their effectiveness in detecting acetaldehyde using analytical techniques. The developed colorimetric microfluidic sensor presents a novel and viable approach for acetaldehyde detection in human urine samples, offering insights into advanced analytical tools for monitoring environmental health and safety.[25,26]

In this investigation, a novel paper-based microfluidic matrix was created using fiber glass paper, offering a unique platform for acetaldehyde analysis. These microfluidic devices operate *via* a color change mechanism, enabling the naked-eye detection of target molecules, while UV spectrophotometers provide quantitative analysis. The utilization of fiber glass paper in manufacturing microfluidic wafers facilitates the detection of acetaldehyde using analytical techniques. The findings from this study demonstrate that the application-based colorimetric microfluidic sensor presents a novel and viable approach for detecting acetaldehyde in human urine samples. The alterations in color and absorbance spectrum resulting from the interaction between the marker and acetaldehyde underscore the capability of the developed method to quantify acetaldehyde in authentic specimens. Moreover, this research marks the initial utilization of AuNPs for the precise and sensitive detection of acetaldehyde in natural samples, offering insights into advanced analytical tools and measurement platforms for acetaldehyde and other volatile organic compounds (VOCs). The simplicity, affordability, and portability of data-oriented microfluidic devices make them a promising option for tracking and monitoring acetaldehyde levels, contributing to enhanced environmental health and safety measures. The success of this colorimetric technique, combined with the simplicity and reliability of microfluidic devices, positions it as a potential off-the-shelf apparatus for widespread application in monitoring acetaldehyde.

It sets the stage for experimentation and observation. To enhance clarity, the process of synthesizing and applying an optical probe for the identification of acetaldehyde is illustrated in Scheme 1.

2. Experiment

2.1 Chemicals and materials

Acetaldehyde, formaldehyde, TMB (3,3′,5,5′-tetramethylbenzidine), NaOH (sodium hydroxide), HCl (hydrogen chloride), $AgNO_3$ (silver nitrate), HAu chloroauric acid, cysteamine (CysA), TSC (trisodium citrate, $Na_3C_6H_5O_7$), PVP K-30 (polyvinylpyrrolidone), DDT (dichlorodiphenyltrichloroethane), acetone, ethanol, hexane, $NaBH_4$ (sodium boro2tide (0), H%), HEPES (4-(2-hydroxyethyl)-1-piperazineethanesulfonic acid), K_2CO_3 (potassium carbonate), CTAB (cetyltrimethylammonium bromide) were obtained from Sigma-Aldrich (Ontario, Canada). Glass fiber was purchased from Whatman Company (Maid Stone, England).

2.2 Instrumentation

Examined the size of nanoparticles using atomic force microscopy (AFM) in tapping mode and Nanosurf (AG Gräubernstrasse 124 410 Liestal Switzerland). Surface area and size were also evaluated by zeta measurement, Zetasizer Ver.7.11 and, dynamic light analysis (DLS) (Malvern Instruments Ltd, MAL1032660, UK). Energy dispersive spectroscopy (EDS) was utilized to measure the composition of the nanoparticles, and the best resolution of scanning electron microscopy (FE-SEM, Hitachi-Su8020, Czech Republic-operating voltage 3 kV) was used to measure the source. The size and morphology of the synthesized nanoparticles were analyzed by transmission electron microscopy (TEM) (Adelaide, Australia, operating voltage 200 kV). EDS is used to analyze the content of nanoparticles. Optical analysis was examined using a UV-visible spectrophotometer Shimadzu UV-1800 with 1 nm resolution.[27]

2.3 Synthesis of AuNPs with different sizes and morphologies

Gold nanoflowers (AuNFs), gold nanoparticles coated with CysA and DDT (AuNPs-CysA/AuNPs-DDT), and gold nanostars (GNSs) were synthesized according to our previous reports.[28–31]

2.3.1 Synthesis of positively charged gold nanoparticles (PCAuNPs). For this purpose, 10 ml of warm HPLC water, agitated at 40 °C, was combined with 50.0 μl of (0.1 M) $NaAuCl_4$

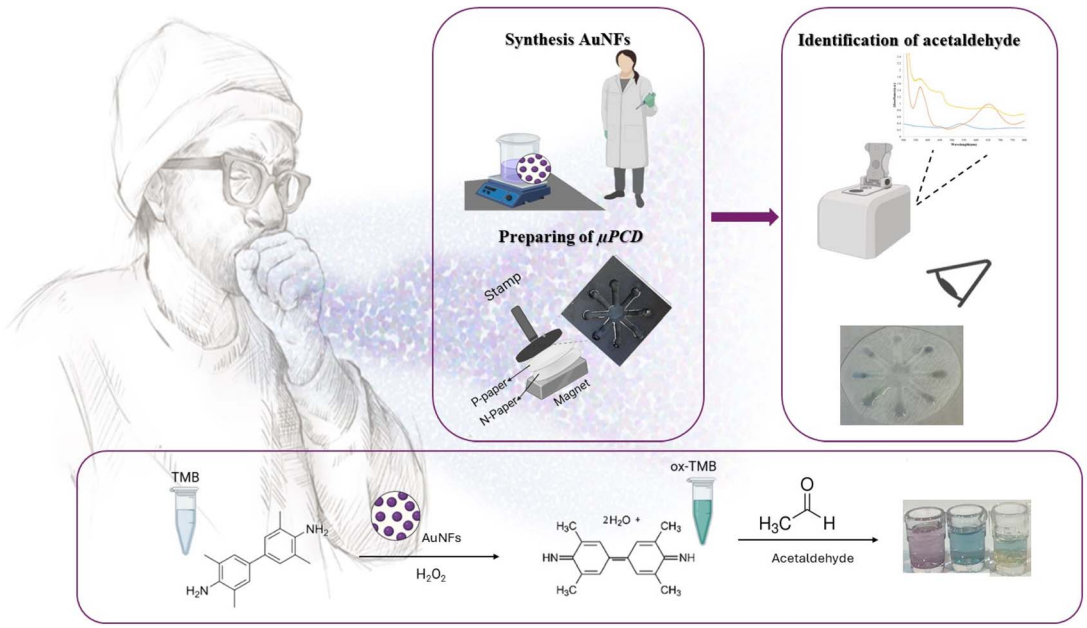

Scheme 1 Synthesis and application of optical probe conjugated with TMB + H_2O_2 to identification of acetaldehyde by μPCD.

and 50.0 μl of ascorbic acid solution (24.0 mg ml^{-1}) to create positively charged gold nanoparticles. As the PCAuNPs developed, the color progressively turned to black. For characterization, the resulting gold nanoparticles were suspended in water after being centrifuged for nine minutes at 5000 rpm.

2.4 Identification of acetaldehyde by proposed optical chemosensor

For this purpose, using optical methods, various AuNPs with different morphologies and sizes were used as probes and mixed with a combination of bluish green TMB and H_2O_2 solution (volume ratio 1 : 1 V/V). The TMB solution is oxidized in the presence of H_2O_2, and with the addition of AuNPs, the NPs act as peroxide and change the color of the solution. Finally, with the addition of the test chemical (acetaldehyde) at room temperature, the color of the chemical changes due to oxidation. The color change was confirmed by UV-visible spectrophotometry as an identification system in the wavelength range of 200–800 nm. For colorimetric analysis, the color change in the solution is monitored with a mobile phone camera and, identification paper is used in the lighting environment.

2.5 Construction of one-droplet microfluidic glass fiber-based device (OD-μPCD)

The OD-μPCD was constructed using a novel method aimed at generating a useable color response from samples in a cost-effective and user-friendly manner. According to our previous publications,[27,29,32] fiberglass papers were immersed in molten paraffin for 30 seconds, followed by removal and allowing the paraffin to dry on the paper for 1 minute. Subsequently, the paraffin-free paper was placed beneath the paraffin-coated paper on the surface of a robust magnet. An 8-pronged iron pattern, heated to 150 °C for 5 minutes and completely hot, was then utilized as a stamp on the papers. The interaction between the magnet and the iron pattern facilitated the creation of hydrophilic channels and hydrophobic areas on the paraffin-free paper.

3. Results and discussion

3.1 Characterization of NPs

In this study, we have included the nanoparticles' characterization information, which were originally presented in our previous publication.[29,31,33–41]

3.2 Qualitative study (naked-eye and spectrophotometry analysis)

AuNPs demonstrate remarkable structure, surface, and photonic characteristics, which have generated significant interest for their utilization in optical chemical sensors. Nanomaterials are widely acknowledged for their physical and chemical attributes, particularly their surface area/volume ratio.[34] The interaction between AuNPs and light gives rise to a phenomenon termed localized surface plasmon resonance, which is distinctive to metal nanoparticles, notably AuNPs.[35] The exceptional optical properties of AuNPs make them well-suited for quick and uncomplicated measurements.[36] Given their unique properties, AuNPs are ideal for integration into optical devices to enable the detection of specific analytes. The findings indicated a decrease in the absorbance intensity of AuNPs-CysA after incubation with TMB + H_2O_2 and TMB + H_2O_2 + acetaldehyde.

In contrast, AuNPs-CysA alone demonstrates negligible exchange rate, highlighting the effectiveness of the nanoparticles on the monitoring of candidate target. It is paved that metal nanoparticles and other nanomaterial-driven chemical

sensors exhibit diverse physical and chemical characteristics.[37] The specific product's functionality is closely linked to the surface area-to-volume ratio.[38] When nanoscale systems interact with light, various processes such as transmission, absorbance, reflection, light scattering, and fluorescence take place.[39] AuNPs boast exceptional structural, surface, and photonic properties, capturing attention as optical devices. Nanomaterials are widely acknowledged for their physical and chemical properties, directly influenced by their environment.[40] The interaction between light and AuNPs leads to the emergence of localized surface plasmon resonance,[35] a phenomenon distinctive to metal nanoparticles, particularly AuNPs. This phenomenon is contingent on the dielectric constant of the surrounding medium.[36] The luminescence effect known as a surface plasmon absorbance band arises from the presence of free electrons in AuNPs. This phenomenon occurs when the accumulation of electron nanoparticles resonates with light. AuNPs exhibit remarkable optical properties, making them ideal for quick and uncomplicated measurements.[38]

The enlargement of AuNP size leads to a shift of the plasmonic absorbance towards longer wavelengths, producing a red light. Moreover, the widening of the absorbance peak indicates the expansion of the suspension and the formation of aggregates.[41] AuNPs play a significant role in numerous drug reactions due to their high surface area-to-surface ratio.[42] The optical characteristics of AuNPs with different morphologies have been extensively examined to enable the identification of analytes through UV-visible spectroscopy.[43] Capping agents or stabilizers are employed to avert the binding or aggregation of AuNPs with other compounds. The application of coating nanoparticles with additives induces electrostatic repulsion, which contributes to their stability.[44] The distinct attributes of AuNPs make them suitable for integration into optical devices for the purpose of detecting specific analytes.[45] Explore of chemosensory behavior in AuNPs-CysA: Here, we utilized cysteamine-modified gold nanoparticles (AuNPs-CysA) as a probe for the detection of acetaldehyde (0.1 μM). The catalytic activity of AuNPs-CysA increased the oxidation rate of TMB. The mobility of small colloidal particles enhances the absorbance of visible light.[46] Stabilizers are utilized to prevent nanoparticles from binding or forming compounds with other materials. As previously mentioned, the application of additives to coat nanoparticles enhances their stability by generating electrostatic repulsion. The negative charge present on the surface of nanoparticles contributes to their unique attributes. The interaction between acetaldehyde and the modified probe causes the accumulation of AuNPs-CysA in the solution, resulting in a change in color and UV-visible spectral wavelengths.

AuNPs can be easily tailored on their surface by attaching functional molecules like cysteamine (CysA) to establish specific binding sites for target molecules. This research investigates the interplay of AuNPs-CysA with acetaldehyde in the presence of TMB + H_2O_2. As depicted in Fig. 1A, the presence of acetaldehyde in the solution induces a shift in the resonance of AuNPs-CysA, leading to a change in the absorbance peak from 520 nm to 655 nm on the UV-visible spectrum. The interaction between acetaldehyde and AuNPs-CysA is

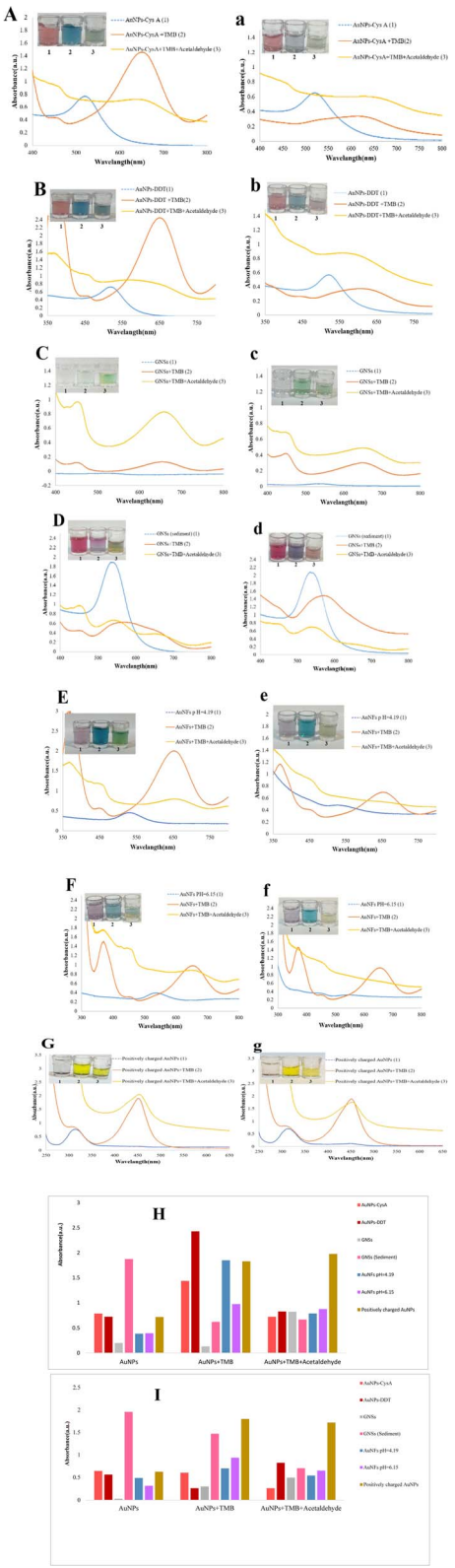

Fig. 1 (A–G) UV-vis absorbance response difference of AuNPs prepared in a mixture of acetaldehyde and a colorless solution, (a–g) images and UV-vis absorbance of the solution after one hour of preparation. (H) Histogram of the absorbance of AuNPs followed by their wavelengths immediately after the reaction with acetaldehyde, (I) in one hour.

predicated on the generation of a Schiff base between the amino group of acetaldehydes and the thiol group of CysA, resulting in the accumulation of AuNPs-CysA in the solution. The binding of AuNPs-CysA to acetaldehyde was ascertained by measuring the absorbance at 550 nm, which increased proportionately with the acetaldehyde concentration. To enhance the detection sensitivity of the AuNPs-CysA-based sensor, TMB was employed as a redox reagent. In the presence of acetaldehyde, AuNPs-CysA facilitates the oxidation of TMB by H_2O_2, causing the color to transition from colorless to green. This green shade is attributed to the formation of the oxidized form of TMB, exhibiting a characteristic peak at 650 nm in the UV-visible spectrum. The intensity of this peak is directly proportional to the concentration of acetaldehyde in the solution. Overall, the interplay among AuNPs-CysA, acetaldehyde, and TMB furnishes a precise and selective technique for the detection of acetaldehyde in a diverse array of samples, encompassing indoor air, food, and biological fluids. In addition, the stability and performance of the chemical sensor are evaluated after one hour. Fig. 1A shows that the absorption density of AuNPs-CysA in the presence of TMB containing and acetaldehyde decreased. In comparison, the exchange rate of AuNPs-CysA alone is negligible, indicating the effectiveness of the nanoparticles.

3.2.1 AuNPs-DDT. Dichlorodiphenyltrichloroethane is a widely used capping agent for AuNPs that provides stability and prevents aggregation of nanoparticles. The results in Fig. 1B show that after adding acetaldehyde to AuNPs and TMB + H_2O_2 solutions, the color changed from red to green and the absorbance peak was shifted from 510 nm to 606 nm. This color change is due to the aggregation of the AuNPs caused by acetaldehyde, which leads to a shift in the red absorbance band.[29] The aggregation of AuNPs induced by acetaldehyde relies on the depletion of the DDT layer on the surface of the nanoparticles. This depletion weakens the steric stability, ultimately resulting in the aggregation of the nanoparticles. In the presence of TMB, a fascinating phenomenon unfolds. AuNPs, alongside DDT, serve as catalysts for the oxidation of TMB by H_2O_2. This catalytic reaction leads to a mesmerizing color shift, transforming the initial red hue to a captivating shade of blue. The movement of the absorbance peak from 504 nm to 657 nm serves as a visual indicator of the formation of TMB oxidized products. The underlying mechanism behind this remarkable transformation lies in the reduction of H_2O_2 by the AuNPs. This reduction generates hydroxyl radicals, which then react with TMB to form the magnificent, oxidized products. In conclusion, the AuNPs, adorned with the remarkable DDT, possess exceptional optical properties and surface chemistry. This renders them exquisitely suitable for utilization in colorimetric assays aimed at detecting the presence of acetaldehyde.

The colorimetric response of the AuNPs to acetaldehyde was based on the aggregation and oxidation of the nanoparticles, respectively. According to Fig. 1B, even if the nanoparticles are estimated to have good stability, the system does not have good stability after one hour.

3.2.2 GNS. While GNS possesses remarkable optical properties attributed to its sharp tips and expansive surface area, it does not inherently detect the color of drugs. Thus, detecting analytes using GNS necessitates alternative methods, such as monitoring changes in the UV-visible spectrum. As previously described, TMB + H_2O_2 were used as redox reagent to detect acetaldehyde. When adding TMB + H_2O_2 to the GNS solution, a slight increase in UV-visible light absorbance was observed due to the interaction of TMB with the hot surface. However, no significant change in absorbance was observed after adding acetaldehyde, indicating that the interaction between acetaldehyde and GNS is weak and does not cause considerable color changes or changes in the UV-visible spectrum (Fig. 1C). However, the interaction between acetaldehyde and GNS can cause changes in GNS surface chemistry, which can affect their properties and interactions with other analytes.

Further studies are needed to elucidate the nature of the interaction between acetaldehyde and GNS and improve detection sensitivity. No significant change in UV was observed after one hour for GNSs, GNSs/TMB + H_2O_2, or GNSs/TMB + H_2O_2/acetaldehyde solutions (Fig. 1C); shows that the interaction between acetaldehyde and GNSs does not cause obvious morphological or chemical changes. Although no change was observed, it was determined that interactions occurred on the GNS surface, and as a result, acetaldehyde absorbance happened on the surface.

3.2.3 GNS. GNS detects acetaldehyde by reacting with TMB + H_2O_2. The UV-visible spectrum of GNS (shown in Fig. 1D) exhibits a broad peak near 543 nm, indicating the absence of any visible color. However, with the addition of TMB + H_2O_2, a new peak was observed at 377–458 nm, resulting from the interaction of TMB with the GNS surface. There is no visible color change of the drug due to the addition of acetaldehyde, and its absorbance is close to zero. This observation suggests that the reaction between acetaldehyde and GNS is ineffective in detecting a signal. The absence of color change indicates that the reaction is not associated with significant changes in the morphology or size of the GNS. The absence of a color change after 1 hour indicates that the reaction is completed and there is no further reaction (Fig. 1D).

3.2.4 AuNFs. This study used AuNFs to detect acetaldehyde at two pH levels (4.19 and 6.15). In the presence of TMB, the color of the nanoparticle-containing they turned blue-green, while the color of acetaldehyde and TMB turned light green.

As shown in Fig. 1E and F, the reaction of TMB + H_2O_2 with AuNFs leading to the formation of the Au(I)–TMB complex. The construction of this complex changes the color of the solution to blue-green and increases the absorbance of wavelengths from 521 to 660 nm. In the presence of acetaldehyde, the H_2O_2 produced by the reaction of TMB with HRP is consumed by the acetaldehyde, resulting in less use of H_2O_2 to oxidize AuNFs. For this reason, the color of the drug turns light green. After one hour, no absorbance was visible in the UV-visible spectrum, making the solution colorless (Fig. 1E and F).

3.2.5 Positively charged gold nanoparticles (PCAuNPs). This experiment used PCAuNPs to detect acetaldehyde in the presence of TMB + H_2O_2. As shown in Fig. 1G, the presence of TMB causes the color of the nanoparticles to change from their original state to bright yellow. Additionally, the UV peak is around 2.0 (a.u.). In contrast, with the addition of acetaldehyde

and TMB + H_2O_2, the color of the PC-AuNPs changed to lighter yellow and a UV peak of approximately 0.8 (a.u.). The detection mechanism used in this study is based on the interaction between AuNPs and TMB, and H_2O_2 as redox indicator. Oxidation of TMB by AuNPs leads to forming blue oxidized TMB radical cations. This reaction can be detected by UV-visible spectroscopy. The peak at 307 nm indicates the presence of oxidized TMB. Adding acetaldehyde causes a reaction with oxidized TMB radical cations, decreasing absorbance at 307 nm and a peak shift to 451 nm. The stability of the obtained AuNPs is due to the electrostatic interaction between the material and the detection surface. The black precipitate extracted after the experiment was used for acetaldehyde detection. TMB is used as a reduced factor, which reduces PC-AuNPs and changes their color from black to yellow. This color change is due to the surface plasmon resonance of the nanoparticles being affected by their size, shape, and dielectric environment. Any change in these parameters will cause a change in the absorbance peak of the nanoparticles. After adding acetaldehyde to the solution containing TMB and PC-AuNPs, Au ions on the surface of the nanoparticles undergo a redox reaction with acetaldehyde, forming acetaldehyde free radicals. These radicals reacted with TMB, leading to further reduction of PC-AuNPs and a change in color. The stability of this system is due to the electrostatic interaction between PC-AuNPs and negatively charged TMB molecules, which prevents the NPs from aggregating over time. Image, color and UV visibility spectrum remain stable after one hour of exposure, indicating appropriate stability.

3.3 Analytical study

In this study, we utilized the peroxidative activity of AuNPs to detect acetaldehyde through a colorimetric method. We employed the UV-vis technique to investigate the distribution of acetaldehyde (0.1–10^{-7} M) using the optical probe in the presence of AuNPs and TMB solutions. The absorbance spectra were recorded within the range of 200–800 nm, as shown in Fig. S1(A–G),† and the absorbance/concentration ratio is presented in Fig. S1(a–g).† Critical analytical parameters, such as the linear band characteristic and lower limit of quantitation (LLOQ), were determined by constructing a standard curve based on the absorbance change in the 400–700 nm band at different acetaldehyde concentrations. We observed a central dipole resonance peak at 455, 542, and 655 nm and a color change at high acetaldehyde levels when exposed to UV-visible light. We attributed this phenomenon to the change in AuNPs morphology and the preference for gold atoms deposited on its surface.

In the presence of certain nanoparticles such as AuNPs-CysA and AuNFs, the absorption increases as the concentration decreases, whereas other nanoparticles like AuNPs-DDT and GNSs exhibit a decrease in absorption with decreasing concentration. This phenomenon can be attributed to the interaction of acetaldehyde molecules with these nanoparticles in solution, leading to a change in the local refractive index and a subsequent modulation of the absorbance peak intensity. The surface area-to-volume ratio of smaller nanoparticles is higher compared to larger nanoparticles, resulting in a more pronounced decrease in absorbance efficiency at lower acetaldehyde concentrations on the larger surface area of small AuNPs. Consequently, the decrease in absorbance efficiency of larger AuNPs may be less significant at lower acetaldehyde concentrations when compared to smaller nanoparticles. The size-dependent properties of AuNPs influence the interaction between nanoparticles and acetaldehyde molecules, thereby affecting the observed absorbance energy in the UV-visible light spectrum. Additionally, these interactions often manifest as discernible color changes that can be observed with the naked eye.

For a comprehensive comparison, the relationships and corresponding equations for each nanoparticle are detailed in Table 1.

As shown in obtained results and comparison of data that indicated in Table 1, AuNFs demonstrated the most pronounced color change at pH = 6.15. Also, as shown in Table 2, this design process offers numerous advantages, including portability, disposability, speed, accuracy, convenience, and affordability. One of its primary strengths is the ability to conduct straightforward field tests through direct testing, eliminating the need for pre-testing or measurement tools and manual dexterity. In contrast, other methods discussed in the study are limited by reliance on expertise, laboratory equipment, preclinical samples, repeated trial time, and require more effort to compensate for human error. Thus, the developed system overcomes these limitations and makes research more accessible and valuable for users.

3.4 Analytical evaluation in real sample

Human urine samples were collected from healthy individuals without prior treatment to evaluate the effectiveness of acetaldehyde detection in real samples. These urine samples were mixed with different concentrations of acetaldehyde (ranging from 17.35 to 10^{-7} M) in a 1 : 1 ratio. Our study results showed a positive relationship between the concentration difference and the corresponding colorimetric measurements in human urine samples. This finding demonstrates the success of our research in accurately detecting and measuring acetaldehyde levels in real samples using colorimetric methods. The regression equations illustrating the relationship between the measured optical response and the concentration of

Table 1 Analytical figure of merit of engineered optical chemosensor for determination of acetaldehyde

Type of optical prob	Linear range	LLOQ
AuNPs-CysA	0.1 μM–10 M	0.1 μM
AuNPs-DDT		
AuNFs pH = 4.19		
GNSs	0.1 μM–0.1 M	0.1 μM
GNSs (sediment)		
AuNFs pH = 6.15	1 μM–1 M	1 μM
PCAuNPs	10 μM–1 M	10 μM

Table 2 Comparison analytical results of different methods for the determination of acetaldehyde

Method	Reaction system	Linear range	LOD/LLOQ	Ref.
Electrochemical	MgO-templated carbon (GMgoc)	0.02–0.1 ppm	0.02 ppm	47
	CeO_2–MWCNT nanocomposite	10^{-8} to 10^{-5} M	7.4×10^{-9} M	48
Spectrophotometry	Coenzyme NAD^+	0.33 μM	0.33 μM	49
Spectro electrochemical enzymatic sensor	$K_3[Fe(CN)_6]/K_4[Fe(CN)_6]$	2.13 ± 0.05 mM (white wine) 5.41 ± 0.16 mM (red wine)	1.99 mM (white wine) 5.51 mM (red wine)	50
Amperometric biosensor	Two platinum thin-film electrodes and a hydrophilic polytetrafluoroethylene membrane	1.00–200 μmol l^{-1}	1.00–200 μmol l^{-1}	51
Fluorescence	CPDs-Tb^{3+}	0.04–42.48	0.02 mM	52
Colorimetric/UV-vis	AuNPs-CysA AuNPs-DDT AuNFs pH = 4.19	0.1 μM–10 M	0.1 μM	This work
	GNSs GNSs (sediment)	0.1 μM–0.1 M	0.1 μM	
	AuNFs pH = 6.15	1 μM–1 M	1 μM	
	PCAuNPs	10 μM–1 mM	1 μM	

acetaldehyde enable precise quantification of acetaldehyde levels in urine samples, enhancing the reliability and accuracy of our detection method.

This way, urine is first tested for its shape and UV-visible spectrum. The color change of the urine sample is shown in Fig. S2.† UV-visible spectrophotometry was used to study absorbance. UV-visible light analysis showed that the urine samples exhibited small peaks at wavelengths between 400 and 600 nm. In the case of GNSs, AuNPs-CysA, AuNFs and PCAuNPs as the concentration decreases, the absorbance intensity increases, but the opposite is true for other AuNPs. There is no color change visible in GNS currently. The different behaviors can be attributed to many factors, including the size, and shape of AuNPs and their chemical composition. The surface properties of AuNPs can vary depending on the synthesis method and the functionalization or modification steps involved. These surface features, such as surface charges and functional groups, can affect the absorbance behavior of acetaldehyde. The complexity of the real matrix structure may affect the absorbance behavior and suggest other factors to consider. Colorimetric and UV-visible results demonstrated the reliability and validity of the chemically produced product in detecting acetaldehyde in real urine. Therefore, this optical device could be an efficient and effective measurement platform for detecting acetaldehyde in urine samples.

3.5 Analytical validity

3.5.1 Selective optical detection of acetaldehyde. In our study, we aimed to evaluate the selectivity of the preparation by examining the influence of various factors. We performed experiments by combining different agents (*e.g.*, acetone, ethanol, glucose, and formaldehyde) with the target analyte. The concentration used for the target analyte acetaldehyde was 10 M. The detection agent/indicator (TMB + H_2O_2) and optical probe (AuNPs) were also included in these experiments. As shown in Fig. S3,† changes in absorbance intensity were observed, and the maximum changes were observed in the presence of acetaldehyde, indicating a good correlation between AuNPs and experimental results. When examining the effects of other analytes, changes in the absorbance band peaks were observed, indicating that the changes in absorbance bands are data for different optical probes. The prepared TMB + H_2O_2 containing AuNPs exhibited UV-visible light absorbance at wavelengths of 350, 450, and 650 nm. The first two absorbance bands (350 and 550 nm) correspond to the out-of-plane and in-plane quadrupole resonances of AuNPs, respectively. The 650 nm band can be attributed to the in-plane dipole resonance of AuNPs.

The change in the bipolar resonance peak of AuNPs can be attributed to the change in AuNP morphology and the release of new AuNP atoms on the AuNP surface and is utilized in the wavelength shift model. In the presence of TMB and interference (GLU/ethanol/acetone and acetaldehyde), the absorbance peak at 450 nm increased and the 650 nm band showed an increase in absorbance. The PC-AuNPs showed an absorbance peak at 450 nm, which was significantly affected by interfering substances, especially acetaldehyde. Furthermore, the presence of acetaldehyde caused a visible color change and absorbance peak in the 450 nm range, whereas no noticeable color change was observed in the presence of glucose, ethanol, and acetone. In this case, the appearance of the peak was solely due to the staining effect. Similar patterns were observed for other types of AuNPs, such as AuNF and eluted AuNPs, which performed well. When tested with all types of AuNPs, acetaldehyde outperformed other analytes in terms of selectivity in real urine samples. Obtained graphs in Fig. S3(H and I)† describe the changes in peak observed in the presence of the target drug, indicating a successful oxidation reaction.

Overall, our research demonstrates that different preparations exhibit varying responses to different factors, with acetaldehyde exhibiting the most significant difference.

3.5.2 Selectivity (effect of different AuNPs and the effect of interfering substances). Additional experiments were performed to investigate the selectivity and suitability of chemical sensors for acetaldehyde detection. The study aimed to evaluate the effect of different AuNPs and interfering substances, such as ethanol, acetone, and glucose, on the detection of acetaldehyde using a TMB + H_2O_2 solution as a colorimetric indicator. The study also investigated the effect of these interfering substances on the accuracy of the model. Ethanol, acetone, and glucose were chosen as interfering substances because they can be found in human urine. The trials involved adding these substances to the TMB + H_2O_2 and AuNPs solution to examine their effect on the detection of acetaldehyde.

Interestingly, small changes in the absorbance spectrum are observed due to interfering modes, indicating that the drug sensor selectively controls acetaldehyde even in the presence of interference properties unrelated to the detection mechanism (Fig. S4†). Human urine samples were used to conduct experiments to test the effectiveness of the drug sensor. The results demonstrate the drug's potential for detecting and quantifying acetaldehyde levels in biological processes (Fig. S5†). Additionally, the chemical sensor accurately detects and measures acetaldehyde levels even in real-world conditions (Fig. S6†).

In conclusion, the study showed that the interaction between AuNPs and related products is a powerful choice for chemical sensors to detect acetaldehyde. The sensor selectively controls acetaldehyde even in the presence of interference properties unrelated to the detection mechanism. Human urine testing confirmed the effectiveness and efficiency of the chemical sensor for detecting acetaldehyde. Additionally, we used a paper-based microfluidic system as a powerful diagnostic tool for accurately and rapidly detecting acetaldehyde. This new system combines simplicity and efficiency, monitoring various assays, including chemicals, viruses, and markers. Paper sensors have attracted attention due to their low cost and ease of use, which has led to progress in this research. It is hoped that these sensors will eventually replace laboratory procedures and enable cost-effective measurements.

3.6 Colorimetric determination of acetaldehyde using OD-μPCD

In our study, we utilized fiberglass paper as the substrate for the chemical sensor due to its superior flow characteristics and lower friction compared to other paper substrates. By incorporating microchannels into the design, we were able to facilitate capillary action, promoting efficient liquid flow and ease of measurement. To detect acetaldehyde, we utilized co-embedded AuNPs in the sensor and added TMB + H_2O_2 and acetaldehyde analyte. As depicted in Fig. 2–4, the presence of acetaldehyde was clearly indicated by a noticeable color change. Moreover, after an hour of incubation, the successful fabrication of hydrophilic channels in the paper substrate was confirmed, further attesting to the reliability and robustness of our system.

Based on the UV visibility results, AuNFs at pH 6.15 demonstrated good detection ability and performance across different acetaldehyde concentrations. As a result, we selected AuNFs (pH 6.15) as the most promising material for further investigation with OD-μPAD. To assess the effect of

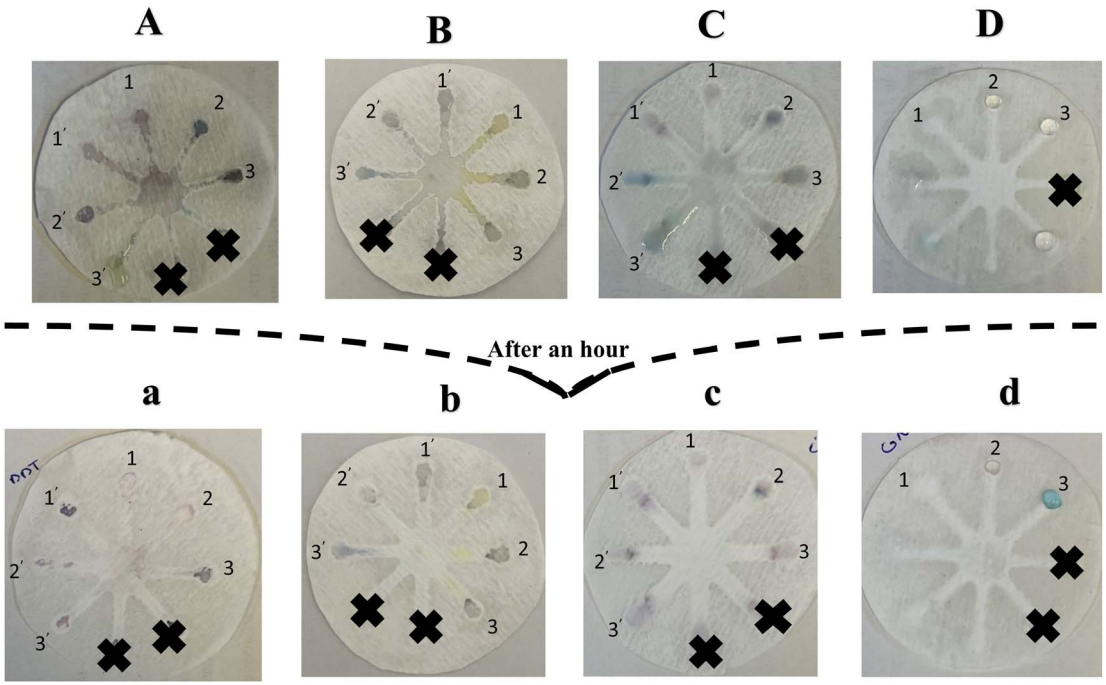

Fig. 2 Photographic images of the fiberglass microfluidic paper-based calorimetric chemosensor for reaction systems: (A) AuNPs-CysA (zone 1–3), AuNPs-DDT (zone 1′–3)′ (a) after 1 hour, and (B) PC-AuNPs (zone 1–3), GNSs (sediment) (zone 1′–3) (b) after 1 hour, (C) AuNFs pH = 6.15 (zone 1–3), AuNFs pH = 4.19 (zone 1–3) (c) after 1 hour, (D) GNSs (zone 1–3), (d) after 1 hour, (1) PC-AuNPs, (2) AuNPs/TMB + H_2O_2, (3) AuNPs/TMB + H_2O_2 + acetaldehyde.

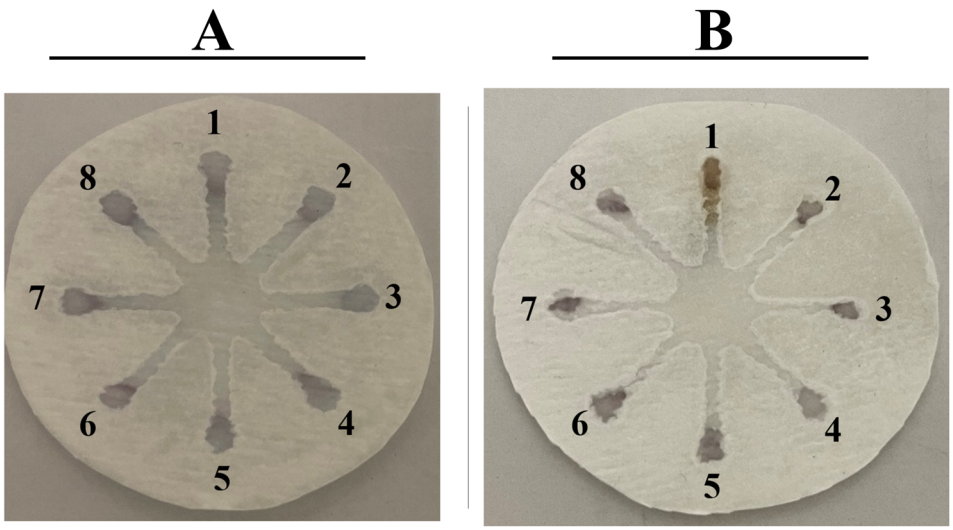

Fig. 3 Photographic images of the (A) different concentration of acetaldehyde and (B) different concentration of acetaldehyde in real sample on the surface of the fiberglass microfluidic paper-based calorimetric chemo sensor.

acetaldehyde concentration in human urine samples, we introduced synthetic AuNFs into the sensing area and observed a noticeable color change upon addition of the test sample (Fig. S7†). This system shows potential as a diagnostic tool for clinical research. Another aspect of our investigation involved measuring the capillary energy of microchannels. By placing

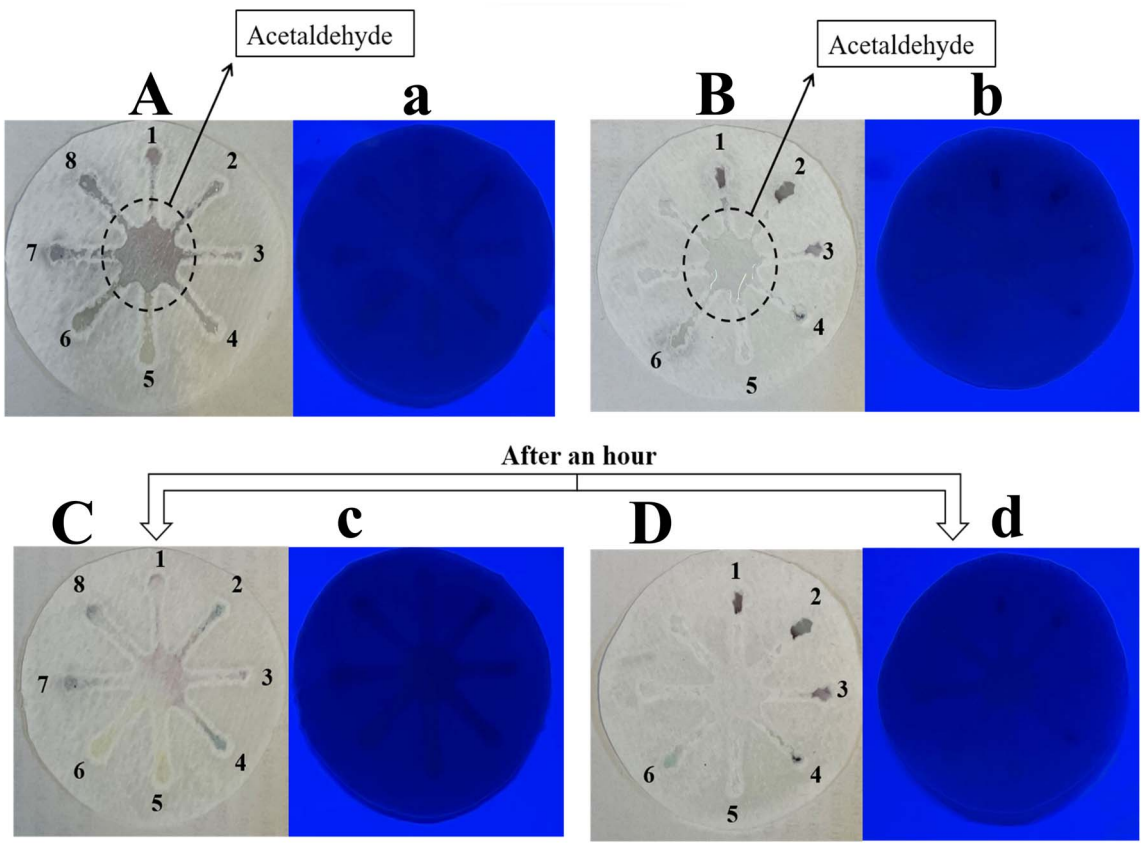

Fig. 4 Photographic images of the fiberglass microfluidic paper-based calorimetric chemo sensor for evaluation of capillary: (A) AuNPs-CysA and colored TMB solution and AuNPs-CysA (zone 1–2), AuNPs-DDT and colored TMB solution and AuNPs-DDT (zone 3–4), positively charged AuNPs and colored TMB solution and PCAuNPs (zone 5–6) and GNSs (sediment) and colored TMB solution and GNSs (sediment) (zone 7–8), (B) AuNFs pH = 6.15 and colored TMB solution and AuNFs pH = 6.15 (zone 1–2), AuNFs pH = 4.19 and colored TMB solution and AuNFs pH = 4.19 (zone 3–4), and GNSs and colored TMB solution and GNSs (zone 5–6). (C and D) photographic images of prepared paper after an hour. (a–d) Colorimetric detection of capillary method under UV light.

AuNFs (probes) and TMB + H_2O_2 in the detection zones and 50 μl of acetaldehyde (analyte) in the sensor area, we observed a lack of color due to redox reactions over time, affirming successful construction of μPADs and drug-sensing substrates with high efficiency, friction-free, and flow rates. We conducted meticulous evaluations of several relevant operators to ensure selection of appropriate chemical sensors. This involved combining relevant products such as acetone, ethanol, glucose, and acetaldehyde with dyes and AuNPs and careful analysis of the results.

The stability of microfluidic preparations was also investigated in this study. The results demonstrated that the system effectively analyzed the acetaldehyde over a period of three days, marking a notable achievement for microfluidic biosensors, particularly considering their early developmental stage. To achieve this, we utilized OD-μPADs for colorimetric analysis of target ions *via* immersion optical probes. After drying at room temperature, the AuNPs combine and turn the color of the paper substrate light purple, with the drying and mixing process taking approximately 10 minutes. This marked the beginning of the development of a nanoparticle-modified OD-μPADs for rapid and accurate identification of acetaldehyde.

The concentration (index) of nanoparticles in the cellulose fibers of the paper, the shape of the paper, and the location of the nanoparticles affect the optical and physical interaction between nanoparticles and the paper substrate. The penetration and accumulation of nanoparticles into the porous structure of the paper cause a change in light compared to the non-porous structure. To preserve their optical properties, it is essential to maintain the solid state of nanoparticles during drying and aggregation.

Our study is the first to successfully utilize OD-μPAD for accurate and powerful identification of acetaldehyde by using AuNPs. To the best of our knowledge, no previous research has employed this method for such purposes. Furthermore, this model exhibits potential for identification of other analytes, including amino acids. The OD-μPAD's low cost and convenience, coupled with its small size, make it a highly portable alternative to larger, more expensive laboratories with specialized operator.

In summary, our study demonstrates significant scientific implications for utilizing AuNPs in microfluidic systems to sensitive detection of acetaldehyde in real samples. The use of microfluidic devices allows for efficient and affordable maintenance analysis. By thoroughly examining specific chemical properties, we showcase the impact of interfering properties on the absorbance spectra of AuNPs. It's important to highlight that the selection and effectiveness of AuNPs are contingent on the type of AuNPs and the interfering agent used in this study.

4. Conclusion

In this study, we developed an enhanced colorimetric method combined with UV-visible spectroscopy for the detection of acetaldehyde in real samples. By employing gold nanoparticles (AuNPs) with varied sizes and morphology, we achieved real-time and selective detection of acetaldehyde amidst diverse interferents. The interaction between acetaldehyde and AuNPs induced significant changes in the absorbance spectrum, enabling rapid and reliable measurement of acetaldehyde concentration. This innovative approach represents a novel application of AuNPs for specific and sensitive acetaldehyde detection in human samples. The microfluidic device utilized in our study offers simplicity, affordability, and portability, rendering it suitable for widespread *in situ* and *ex situ* acetaldehyde monitoring in environmental, industrial, and biomedical settings. Moreover, engineered one-drop microfluidic colorimetric devices (OD-μPCDs) demonstrate excellent stability for long-term storage and analysis, making them indispensable for field applications and remote sensing. The advanced colorimetric method, coupled with the simplicity and reliability of the microfluidic format, can be readily commercialized as a user-friendly device. By replacing conventional laboratory techniques with the innovative approach proposed in this study, we anticipate enhanced accessibility to acetaldehyde analysis for environmental organizations, manufacturers, and medical facilities. Continued refinement and exploration of this approach holds the potential to enhance its performance, broaden its applicability to other compounds, and address new challenges in chemical analysis. We envision that our work will inspire further research and contribute to the development of superior technology for detecting and monitoring acetaldehyde on a global scale.

In summary, our study represents a significant breakthrough in colorimetric detection, highlighting the promise of AuNPs and paper-based microfluidics for sensitive and selective acetaldehyde analysis. This work lays the foundation for future advancements in analytical chemistry, facilitating rapid and accurate measurement of acetaldehyde exposure to bolster environmental, health, and safety standards. Further exploration and refinement may enhance the effectiveness of this approach, extend its suitability for other substances, and tackle emerging challenges in chemical analysis. Overall, our study marks a noteworthy progression in color detection, showcasing the potential of AuNPs and paper-based microfluidics for precise and selective detection of acetaldehyde, while serving as a platform for advancing the detection of acetaldehyde and other volatile organic compounds (VOCs) across diverse regions.

Conflicts of interest

There are no conflicts to declare.

Acknowledgements

We gratefully acknowledge the pharmaceutical analysis Research Center, Tabriz University of Medical Sciences for instrumental supporting of this research (Grant No. 73702).

References

1 F. O. Adeola, *Handbook of Global Health*, 2020, pp. 1–30.
2 J. J. Baert, J. De Clippeleer, L. De Cooman and G. Aerts, *J. Am. Soc. Brew. Chem.*, 2015, **73**, 100–108.

3 J. I. Garaycoechea, G. P. Crossan, F. Langevin, L. Mulderrig, S. Louzada, F. Yang, G. Guilbaud, N. Park, S. Roerink and S. Nik-Zainal, *Nature*, 2018, **553**, 171–177.
4 K. C. Zenki, B. H. M. Mussulini, E. P. Rico, D. L. de Oliveira and D. B. Rosemberg, *Toxicol. in Vitro*, 2014, **28**, 822–828.
5 H. Lin, H. Jiang, S. Y.-S. S. Adade, W. Kang, Z. Xue, M. Zareef and Q. Chen, *Crit. Rev. Food Sci. Nutr.*, 2023, **63**, 8226–8248.
6 Y. Liu, C. Liu, X. Xu, C. Niu, J. Wang, F. Zheng and Q. Li, *Foods*, 2022, **11**, 3450.
7 S. S. H. Ho and J. Z. Yu, *Environ. Sci. Technol.*, 2004, **38**, 862–870.
8 R. P. Dator, M. J. Solivio, P. W. Villalta and S. Balbo, *Toxics*, 2019, **7**, 32.
9 Q. A. Drmosh, I. Olanrewaju Alade, M. Qamar and S. Akbar, *Chem.–Asian J.*, 2021, **16**, 1519–1538.
10 M. M. Rahman, S. B. Khan, M. Faisal, A. M. Asiri and K. A. Alamry, *Sens. Actuators, B*, 2012, **171**, 932–937.
11 B. L. Gray, *IEEE Nanotechnol. Mag.*, 2014, **8**, 6–16.
12 N. Maluf and K. Williams, *An Introduction to Microelectromechanical Systems Engineering*, Artech House, 2004.
13 M. Razmkhah, S. Abtahi and A. Ghaderi, *Curr. Stem Cell Res. Ther.*, 2019, **14**, 43–51.
14 V. Rincón Montes, PhD dissertation, RWTH Aachen University, 2021.
15 V. N. Ataide, L. F. Mendes, L. I. Gama, W. R. de Araujo and T. R. Paixão, *Anal. Methods*, 2020, **12**, 1030–1054.
16 K. Nejati, M. Dadashpour, T. Gharibi, H. Mellatyar and A. Akbarzadeh, *J. Cluster Sci.*, 2021, 1–16.
17 H. Jans and Q. Huo, *Chem. Soc. Rev.*, 2012, **41**, 2849–2866.
18 K. Kelly, E. Coronado and L. L. Zhao, *J. Phys. Chem. B*, 2003, **107**, 668–677.
19 X. Bai, Y. Wang, Z. Song, Y. Feng, Y. Chen, D. Zhang and L. Feng, *Int. J. Mol. Sci.*, 2020, **21**, 2480.
20 P. Nosovitskiy, G. Nosovitskiy, K. Nandigam, R. Abozaid and S. Karan, in *Breath Analysis: an Approach for Smart Diagnostics*, Springer, 2022, pp. 161–200.
21 C.-W. Tsao, *Micromachines*, 2016, **7**, 225.
22 X. Qin, J. Liu, Z. Zhang, J. Li, L. Yuan, Z. Zhang and L. Chen, *TrAC, Trends Anal. Chem.*, 2021, **143**, 116371.
23 H. Canbolat, *IEEE Trans. Instrum. Meas.*, 2009, **58**, 3762–3768.
24 J. B. Nielsen, R. L. Hanson, H. M. Almughamsi, C. Pang, T. R. Fish and A. T. Woolley, *Anal. Chem.*, 2019, **92**, 150–168.
25 K. Mahato, A. Srivastava and P. Chandra, *Biosens. Bioelectron.*, 2017, **96**, 246–259.
26 E. Noviana, T. Ozer, C. S. Carrell, J. S. Link, C. McMahon, I. Jang and C. S. Henry, *Chem. Rev.*, 2021, **121**, 11835–11885.
27 F. Farshchi, A. Saadati, M. Hasanzadeh, Y. Liu and F. Seidi, *RSC Adv.*, 2023, **13**, 6225–6238.
28 A. Mobed, F. Kohansal, A. Ahmadalipour, M. Hasanzadeh and F. Zargari, *Anal. Methods*, 2021, **13**, 311–321.
29 F. Farshchi, A. Saadati, M. Hasanzadeh and F. Seidi, *RSC Adv.*, 2021, **11**, 27298–27308.
30 N. Razmi, M. Hasanzadeh, M. Willander and O. Nur, *Anal. Methods*, 2022, **14**, 1562–1570.
31 S. Ahmadi, Z. Ghasempour and M. Hasanzadeh, *Food Chem.*, 2023, **423**, 136307.
32 A. Saadati, F. Farshchi, M. Jafari, H. Kholafazad, M. Hasanzadeh and N. Shadjou, *RSC Adv.*, 2024, **14**, 8602–8614.
33 A. Saadati, F. Farshchi, M. Hasanzadeh and F. Seidi, *Anal. Methods*, 2021, **13**, 3909–3921.
34 H. Yin, H. Too and G. Chow, *Biomaterials*, 2005, **26**, 5818–5826.
35 J. A. Delaire and K. Nakatani, *Chem. Rev.*, 2000, **100**, 1817–1846.
36 A. E. Miroshnichenko, S. Flach and Y. S. Kivshar, *Rev. Mod. Phys.*, 2010, **82**, 2257.
37 A. Sharma, Y. Zhu, E. J. Spangler and M. Laradji, *J. Chem. Phys.*, 2022, **156**, 4689–4698.
38 V. Amendola, R. Pilot, M. Frasconi, O. M. Maragò and M. A. Iatì, *J. Phys.: Condens. Matter*, 2017, **29**, 203002.
39 H. E. Toma, V. M. Zamarion, S. H. Toma and K. Araki, *J. Braz. Chem. Soc.*, 2010, **21**, 1158–1176.
40 F. Flory, L. Escoubas and G. Berginc, *J. Nanophotonics*, 2011, **5**, 052502.
41 N. E. Larm, J. B. Essner, K. Pokpas, J. A. Canon, N. Jahed, E. I. Iwuoha and G. A. Baker, *J. Phys. Chem. C*, 2018, **122**, 5105–5118.
42 P. Boomi, R. Ganesan, G. Prabu Poorani, S. Jegatheeswaran, C. Balakumar, H. Gurumallesh Prabu, K. Anand, N. Marimuthu Prabhu, J. Jeyakanthan and M. Saravanan, *Int. J. Nanomed.*, 2020, 7553–7568.
43 E. C. Dreaden, A. M. Alkilany, X. Huang, C. J. Murphy and M. A. El-Sayed, *Chem. Soc. Rev.*, 2012, **41**, 2740–2779.
44 S. Zeng, D. Baillargeat, H.-P. Ho and K.-T. Yong, *Chem. Soc. Rev.*, 2014, **43**, 3426–3452.
45 E. Borgarello, J. Kiwi, M. Graetzel, E. Pelizzetti and M. Visca, *J. Am. Chem. Soc.*, 1982, **104**, 2996–3002.
46 B. Metz, G. F. Kersten, P. Hoogerhout, H. F. Brugghe, H. A. Timmermans, A. De Jong, H. Meiring, J. ten Hove, W. E. Hennink and D. J. Crommelin, *J. Biol. Chem.*, 2004, **279**, 6235–6243.
47 I. Shitanda, T. Oshimoto, N. Loew, M. Motosuke, H. Watanabe, T. Mikawa and M. Itagaki, *Biosens. Bioelectron.*, 2023, **238**, 115555.
48 R. M. Shereema, S. R. Nambiar, S. S. Shankar and T. P. Rao, *Anal. Methods*, 2015, **7**, 4912–4918.
49 H. Zhu, R. Gonzalez and T. A. Bobik, *Appl. Environ. Microbiol.*, 2011, **77**, 6441–6450.
50 D. Ibáñez, M. B. González-García, D. Hernández-Santos and P. Fanjul-Bolado, *Biosensors*, 2022, **12**, 1032.
51 T. Gessei, T. Arakawa, H. Kudo, H. Saito and K. Mitsubayashi, *Anal. Lett.*, 2014, **47**, 1361–1374.
52 R. Guan, S. Zhang, X. Fan, X. Shao, Y. Hu, T. Liu, S. Wang and Q. Yue, *J. Fluoresc.*, 2022, **32**, 759–770.